SHAPE ADAPTIVE GRINDING (SAG) OF COMPLEX ADDITIVELY MANUFACTURED PARTS

Anthony T. Beaucamp[1], Yoshiharu Namba[1], Phillip Charlton[2], Samyak Jain[2], Arthur A. Graziano[2]
[1]Department of Mechanical Engineering, Chubu University, Kasugai, Aichi, Japan
[2]Zeeko Ltd, Coalville, Leicestershire, UK

INTRODUCTION

Electron beam melting (EBM) [1-2] and selective laser sintering (SLS) [3] are cutting-edge additive manufacturing (AM) processes used to produce three dimensional shapes by melting metal powder layer by layer. These technologies have recently become widely adopted in applications such as dental and prosthetic implants, or the prototyping of aeronautical components such as shown in Figure 1 [4-5].

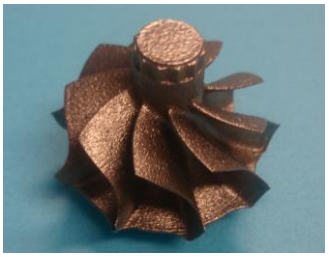

FIGURE 1. Example of "complex" rapidly prototyped component.

The final surface roughness produced by AM however, is unsatisfactory for many applications, demanding a post-finishing process to improve the surface quality prior to usage. One such method involves conformal grinding and polishing of complex additively manufactured shapes such as aero-engine blisks, but usually only achieve roughness around 0.5 µm *Ra* [6]. Although current finishing methods may have a distinct advantage, such as being able to finish porous structures, their resulting surface roughness is still limited. To expand on AM's many applications, it is necessary to further improve the surface roughness of components while limiting the number of finishing operations.

In this paper, we introduce a novel process called Shape Adaptive Grinding (SAG) that combines an elastically compliant tool with small grinding pellets. The process was applied to post-processing of titanium alloy (Ti6Al4V) additively manufactured by EBM and SLS.

SHAPE ADAPTIVE GRINDING

The shape adaptive grinding (SAG) process builds upon the precessed bonnet concept whereby an inflated, spherical, membrane tool is used to machine a surface at a tilted (precessed) orientation [7]. This bonnet (elastic tool) is typically covered with a polishing cloth, and a stream of abrasive slurry is constantly supplied to the tool. As the bonnet presses against the surface of the workpiece (controlled by the tool-offset), the contact-spot diameter increases.

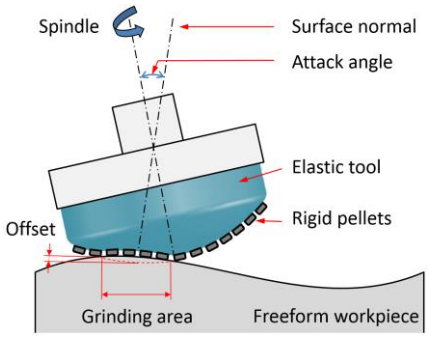

FIGURE 2. Principle of shape adaptive grinding.

However, in the SAG process, instead of being covered with a polishing cloth, the rubber bonnet is covered with nickel bonded (NBD) or resin bonded (RBD) diamond pellets, as shown in Figure 2 [8], with water used as a coolant. The deformability of the elastic layer allows the tool to conform to freeform surfaces featuring any convex or concave curvature larger than about twice the radius of the spherical SAG tool. Simultaneously, at smaller scale, the diamond pellets act as a rigid tool and allow for grinding to take place. The result is a shape adaptive grinding process with the benefits of both polishing and grinding techniques. This allows for greater material removal than standard polishing techniques, while achieving low surface roughness on complex freeform shapes. A 7-axis CNC machine actively controls the spindle speed, attack angle, tool offset, and surface speed of the tool as it traverses the surface of the workpiece; allowing for control of the grinding spot in terms of contact area and removal rate.

STUDY OF GRINDING PROCESS

Experimental procedure

Flat Ti6Al4V samples produced by EBM and SLS were procured in order to perform a series of experiments to determine the range of surface roughness and removal rates achievable with the SAG process. The initial surface roughness of the flat samples ranged between 4 and 5 µm *Ra*.

A series of 5 x 45 mm sub-sections of the titanium sample were ground using the machining parameters shown in Table 1. For the surface roughness experiments, the work spindle was operated at 75% of the maximum speed in order to achieve optimal productivity and to limit the thermal expansion of the spindle (i.e. frictions in the mechanical bearings). Tool pressure of 1.0 bar, attack angle of 20°, and tool offset of 0.3 mm were selected in accordance with previous experience of the SAG process [8]. The tool feed rate was allowed to vary across the sub-sections, with step values of 25, 50, 100, 200, and 400 mm/min. For each sub-section, when the rate of improvement in surface roughness diminished, the optimal feed was recorded. From one sub-section to the next, the nominal size of final diamond abrasives in the SAG pellets was decreased from 40 µm down to 3 µm, until a smooth surface could be obtained.

For the removal rate experiments, another sample of titanium was ground using the machining parameters shown in Table 1, which were selected in accordance with previous experience of the SAG process. The tool feed rate was kept constant in these experiments, and after each grinding pass the removal rate was determined by generating influence spots (dwelling of the tool at a static location).

TABLE 1. Parameters of surface roughness and removal rate experiments.

Parameter	**Surface roughness test**	**Removal rate test**
Shape Material Process	Flat Ti6Al4V EBM and SLS	Freeform SLS
Attack angle Spindle speed Tool pressure Tool offset Raster spacing Surface feed	20° 1500 rpm 1.0 bar 0.3 mm 0.3 mm 25, 50, 100, 200, and 400 mm/min	20° 750 rpm 1.0 bar 0.2 mm 0.21, 0.20, 0.19 mm 200 mm/min
Tool radius Abrasive size Abrasive type	10 mm 40, 9 and 3 µm Diamonds bonded in nickel and resin pellets	

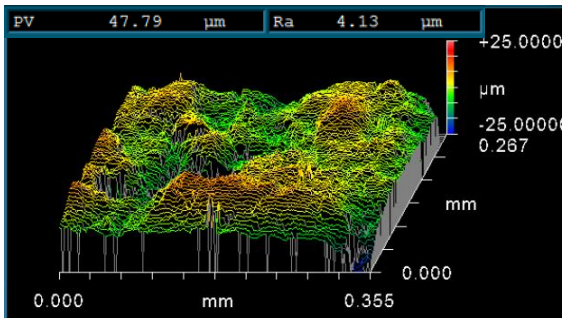

(a) As received

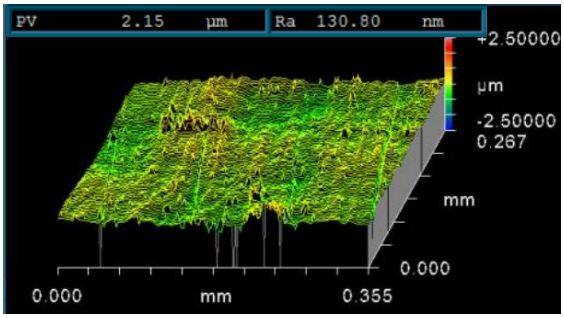

(b) Nickel bonded 40 µm

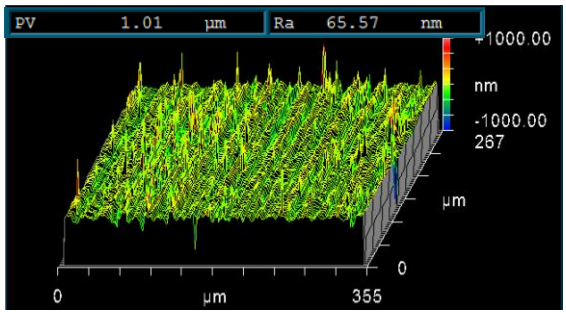

(c) Nickel bonded 9 µm

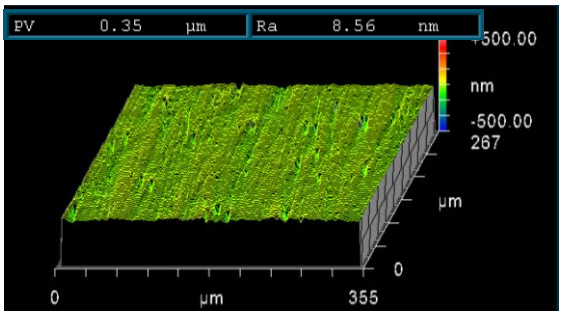

(d) Resin bonded 3 µm

FIGURE 3. 3D measurements of surface at 10x magnification, after successive grinding runs.

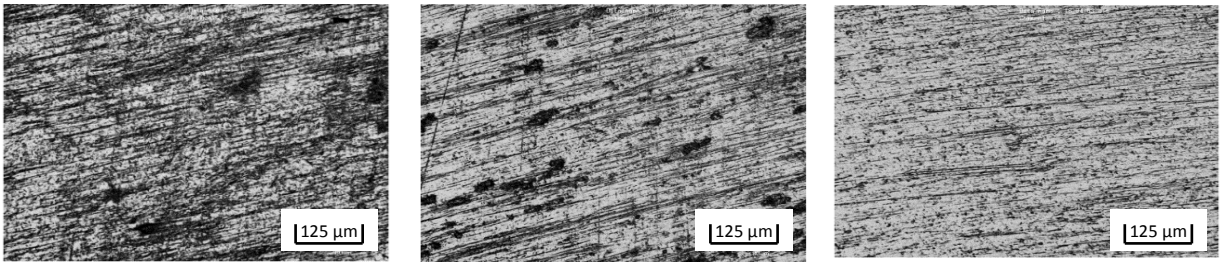

(a) Nickel bonded 40 µm (b) Nickel bonded 9 µm (c) Resin bonded 3 µm

FIGURE 4. Laser microscope images taken at 20X after successive runs.

Surface roughness

Figure 3 shows three-dimensional profiles of the surface taken with a white light interferometer at 10x magnification. Figure 4 shows laser microscope images of the same areas at 20x magnification, after reaching optimal surface roughness on the EBM samples with each SAG tool (progression on the SLS samples was similar). Due to the rough initial condition of the surface, a coarse 40 µm NBD SAG tool was first used to remove the micro-structured surface layer. Figure 3(b) and 4(a) show the resulting surface, in which the structured layer was mostly removed, allowing for finer grinding with subsequent SAG tools.

The next sub-section was prepared by pre-grinding at optimal feed rate with the 40 µm NBD tool. A 9 µm NBD tool was then used. Figure 3(c) and 4(b) show a reduction in the surface micro-structure, but the emergence of a directional surface texture could also be observed. The next sub-section was prepared by pre-grinding with the 40 µm and 9 µm NBD tools at optimal feed. Then, a 3 µm RBD SAG tool was used for final smoothing. The grinding direction was aligned perpendicular to that of the previous 9 µm NBD tool. The final surface shows attenuation of the directional scratches, and low surface roughness below 10 nm *Ra*, as seen in Figure 3(d) and 4(c). These results show substantial improvement by more than one order of magnitude when compared with other methods for post-processing AM titanium.

Figure 5 shows the evolution of surface roughness *Ra* at 10x magnification with successive SAG tools, as a function of grinding time across the 5 x 45 mm sub-sections (the observed surface roughnesses were consistent between EBM and SLS samples). The markers on each spline regression curve, indicate the progressive decrease of feed rate from 400, 200, 100, 50, down to 25 mm/min.

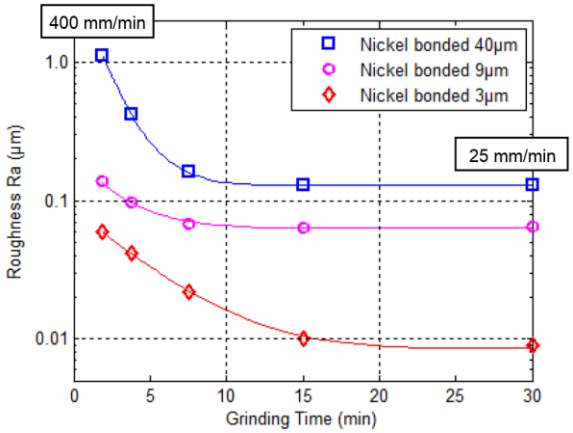

FIGURE 5. Evolution of surface roughness Ra.

Based on these results, it was found that optimal grinding could be obtained by using the following steps: 100 mm/min with 40 µm and 9 µm NBD SAG tools, and 50 mm/min with 3 µm RBD SAG tool (30 min total).

Removal rate

In order to determine the extent to which the SAG process can be used to finish artifacts without degradation of the dimensional accuracy, an accurate estimate of the removal rate must be determined. For this reason, the various SAG tools were used to grind a workpiece for 60 minutes each, and the removal rate was determined every 30 minutes by generating influence spots (dwelling a few seconds at static locations). The spot depth was then measured with a profilometer, and used to compute the equivalent volumetric removal rate, as shown in Figure 6 (the observed removal rates were consistent between EBM and SLS samples, and are plotted here with linear regressions).

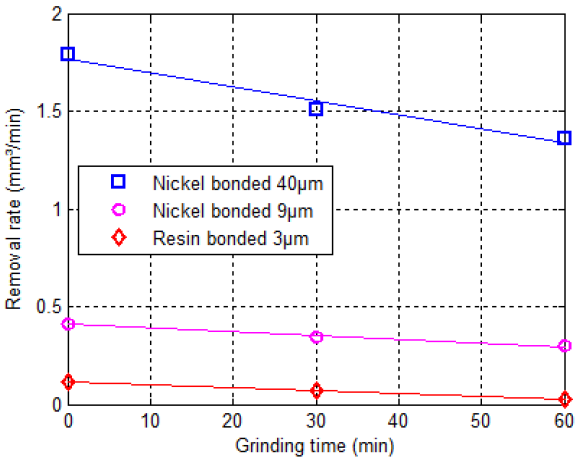

FIGURE 6. Evolution of removal rate as a function of grinding time for each SAG tool.

The volumetric removal rates ranged from about 0.1 mm^3/min for the 3 µm RBD up-to 2 mm^3/min for the 40 µm NBD. The removal rate of the SAG tools was found to follow a linear decline over time, which was consistent from tool to tool. It was found that the removal rate could be scaled up by either increasing the radius of the SAG tools (current SAG tools had 10 mm radius) or manipulating the CNC controller variables such as higher spindle rotation, or increased attack angle.

APPLICATION TO FREEFORMS

Experimental procedure

The application of the SAG process to freeform shapes was demonstrated on an SLS prepared complex sample shown in Figure 7(a). The sample consists of convex, concave, and saddle shaped areas with curvature ranging from 30 mm radius (concave) to 10 mm radius (convex). Figure 7(b) shows a rendering of the corresponding CAD model, with the area to be finished in blue. The SAG grinding process was performed on a 7-axis CNC controlled machine built by Zeeko Ltd.

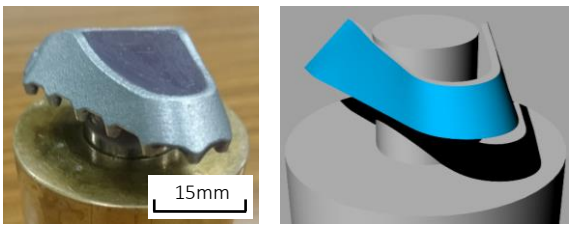

(a) As received (b) Area to be ground (blue)

FIGURE 7. Freeform sample prepared by SLS.

An on-machine probing system was used to characterize and compensate the deviation between CAD model and actual workpiece. A soft probe was mounted on the tool spindle, and used to detect the surface by touch/trigger sensing mode. Figure 8(a) shows a 3D array of points that was used to probe the surface by the machine software. The resulting data was then freeform fitted to the CAD model to determine the workpiece location inside the machine, and the residual form deviation against the CAD model. This data was used to compensate the CNC toolpath.

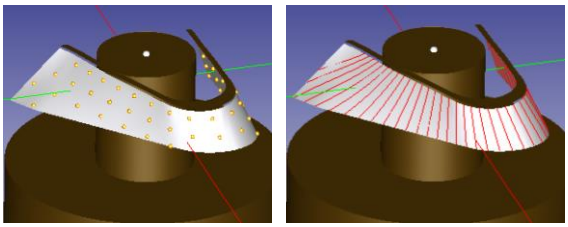

(a) Grid of probe point (b) Tracks of raster path

FIGURE 8. Definition of the probing and toolpath in the CAD/CAM software.

Since the positioning errors of the CNC machine had not been fully calibrated, this method could not be used to provide absolute measurements of the freeform shape. Nevertheless, the probing repeatability was determined to be better than 0.5 µm *rms* prior to the grinding experiments. Therefore, relative changes in the form error could be tracked between grinding runs by subtracting before and after measurements, which provided an estimate of the 3D removal function with an accuracy better than 0.5 µm rms.

In order to produce the toolpath for finishing, the freeform shape was sectioned with a series of planes along the length of the surface to generate the raster path, as seen in Figure 8(b). Three SAG passes were performed with toolpath parameters very similar to those shown in the removal rate section of Table 1.

The process parameters were chosen to produce a toolpath within the dynamic range of the machine. They also reflected the faster processing condition of SLS material compared to EBM. The total grinding time was 45 minutes, consisting of 14 min with 40 µm NBD, 15 min with 9 µm NBD, and 16 min with 3 µm RBD.

(a) As received *(b) SAG machining* *(b) Final condition*

FIGURE 9. Condition of freeform sample after successive grinding runs.

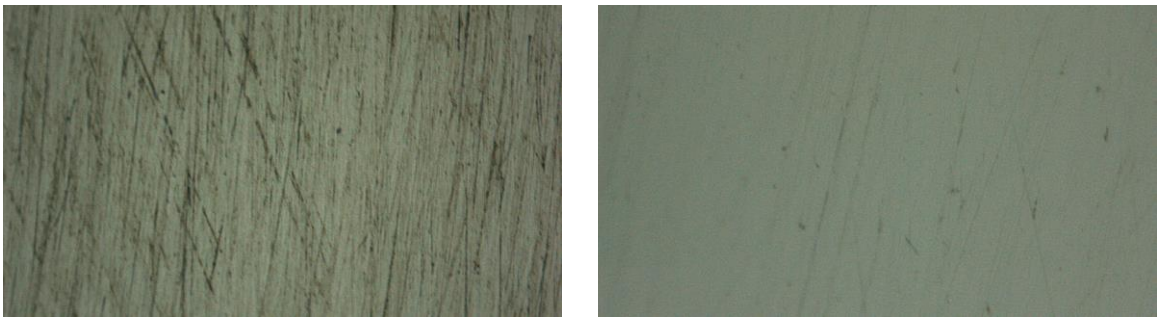

(a) After grinding with resin bonded 3 µm (b) After final polishing with 1 µm diamond paste

FIGURE 10. Optical microscope images of freeform surface taken at 100x magnification.

Surface roughness

Figure 9 shows photographs of the surface before, during, and after grinding. A mirror-like surface was achieved after only 3 SAG grinding runs were performed on the original AM surface condition (with roughness above 5 µm *Ra*). The improvement in surface reflectivity can be easily observed. The surface roughness was measured using white light interferometry to be 12.8 nm *Ra*.

Figure 10(a) shows the resulting surface after the third grinding run by 3 µm RBD (measured at 100x via optical microscope). The residual grinding marks observed after grinding on the freeform surface were very similar to those observed on the flat sample prepared by SLS. It can also be noted that substrates produced by state-of-the-art SLS technology delivered finishing with fewer residual pores than EBM, which would indicate a superior melting condition.

In order to further improve the surface condition, a final smoothing run was performed using the precessed bonnet polishing process, on the same machine and with a bonnet of similar shape and dimension as the SAG tools. A felt polishing cloth was employed together with 1 µm diamond paste. The polishing toolpath parameters were altered slightly: spindle speed of 400 rpm, attack angle 10 degrees, and track spacing 0.18 mm were selected based on previous experience with diamond polishing [9]. After a 17 min bonnet polishing run, the surface was measured again as shown in Figure 10(b). The grinding marks were mostly removed, leaving a very smooth surface with roughness below 3 nm *Ra*.

SUMMARY

The novel shape adaptive grinding process has been applied to post-process surface finishing of titanium alloy (Ti6Al4V) additively manufactured by EBM and SLS. It has been shown that the micro-structured surface layer resulting from the melting process can be removed using nickel

bonded 40 µm and 9 µm diamond SAG tools. The surface can then be further improved to approximately 10 nm *Ra* roughness by finishing with a resin bonded 3 µm diamond SAG tool. Thus, using only 3 different tools, the surface can be improved from 5 µm down to about 10 nm *Ra*; a decrease of almost 3 orders of magnitude. The process is lubricated with water, requiring only a simple tool change between successive runs.

The SAG process was also validated on a freeform sample, thus showing the ability of the tool to adapt to varying curvature from convex to concave. The finishing process maintained a shape deviation of less than +/- 5 µm, which is acceptable when compared to the typical accuracy after additive manufacturing. Finally, further bonnet polishing with diamond abrasives showed that the roughness can be easily brought further down to 3 nm *Ra*.

It was found that SLS samples finished by this process displayed fewer pores than EBM samples, which would indicate that state-of-the-art SLS technology is capable of delivering substrates with better material uniformity than standard EBM technology. The SAG technology is expected to find many applications in the post-process finishing of rapidly prototyped titanium alloy components for such applications as aeronautics and medical components.

ACKNOWLEDGEMENTS

This work was supported by the JSPS Grant-in-Aid for Scientific Research (B) No. 22360063 and the Post-Doctoral program for foreign researchers from the Japan Society for the Promotion of Science. SLS samples were kindly provided by Renishaw plc, and EBM samples by Matthieu Kobilinsky Design.

REFERENCES

[1] Murr L, Gaytan S, Ramirez D, Martinez E, Hernandez J, Amato K. Metal fabrication by additive manufacturing using laser and electron beam melting technologies. Journal of Materials Science and Technology. 2012; 28(1): 1-14.

[2] Cormier D, Harrysson O, West H. Characterization of H13 steel produced via electron beam melting. Rapid Prototyping Journal. 2004; 10(1): 35-41.

[3] Mukesh A, Bourell D, Beaman J, Marcus H, Barlow J. Direct selective laser sintering of metals. Rapid Prototyping Journal. 1995; 1(1): 26-36.

[4] Guo N, Leu M. Additive manufacturing: technology, applications and research needs. Frontiers of Mechanical Engineering. 2013; *8*(3): 215-243.

[5] Chahine G, Koike M, Okabe T, Smith P, Kovacevic R. The design and production of Ti-6Al-4V ELI customized dental implants. Journal of Metals. 2008; 60(11): 50-55..

[6] Duan J, Shi Y, Lin X, Dong T. Flexible Polishing machine with dual grinding heads for aeroengine blade and blisk. Advanced Materials Research. 2011; 317: 2454-2460.

[7] Walker D, Freeman R, Morton R, McCavana G, Beaucamp A: Use of the 'Precessions'™ process for pre-polishing and correcting 2D & 2½D Form. Optics Express. 2006; 14(24): 11787-11795.

[8] Beaucamp A, Namba Y, Combrinck H, Charlton P, Freeman R. Shape adaptive grinding of CVD silicon carbide, Annals of the CIRP. 2014; 63(1): 317-320.

[9] Beaucamp A., Namba Y., Inasaki I., Combrinck H., Freeman R. Finishing of optical moulds to λ/20 by automated corrective polishing, Annals of the CIRP. 2011; 60(1): 375-378.

[10] Gibson I, Rosen D, Stucker B. Additive manufacturing technologies. New York: Springer, 2010.